Bond behavior of FRP Bars under direct pullout conditions

Zenon Achillides [1] and Kypros Pilakoutas[2]

Abstract: This paper examines the behavior of the Eurocrete FRP bars (Glass, Carbon, Aramid and Hybrid) in concrete under direct pullout conditions. More than 130 cube specimens were tested in direct pullout, where no splitting was allowed to develop. In normal concrete, the mode of bond failure of FRP bars was found to differ substantially from that of deformed steel bars, due to damage to the resin rich surface of the bar when pull-out takes place. The bond strengths developed by CFRP and GFRP bars appear to be very similar and just below what is expected from deformed steel bars under similar experimental conditions. The load slip curves highlight some of the fundamental differences between steel and FRP materials.

This paper reports in detail on the influence of various parameters that affect bond strength and development, such as: the embedment length, type, shape, surface characteristics and diameter of the bar as well as the concrete strength. The testing arrangement is also shown to influence the bond strength, due to the "wedging effect" of the bars.

Keywords: bond behavior, bond strength; pull-out test; CFRP, GFRP

1 Dr. Civil Engineer, Univ. of Sheffield, Dept. of Civil and Structural Eng., Sir Frederic Mappin Building, Mappin Street, Sheffield, UK, e-mail: zachillides@hotmail.com

2 Reader, The University of Sheffield, Department of Civil and Structural Engineering, Mappin Street, Sheffield, S1 3JD, UK, e-mail: k.pilakoutas@sheffield.ac.uk

INTRODUCTION

In construction, steel reinforced concrete is the most widely used structural material in the world. However, it is well known that, under certain environments, the corrosion of steel reinforcement can lead to the deterioration or even collapse of structural elements. Billions of dollars are spent every year world-wide in repairing and strengthening concrete structures, whose reinforcement has deteriorated due to corrosion and this has contributed for research to focus on alternative solutions (Pilakoutas, 2000).

FRP materials offer a promising solution since for many years they are successfully used in other industries (such as the automobile and sports manufacturing industries) and more recently in construction. There are many examples of structural applications that have demonstrated that the speed and convenience of strengthening and repairing concrete structures using advanced composites produce cost effective solutions (Head 1996). In addition, structures reinforced with FRP bars have been in service under aggressive environments in various parts of the world, for more than 15 years, without any structural problems (Rostasy, 1996).

Nevertheless, before FRP materials are widely accepted in construction industry, research has to be done on all aspects of their structural behavior. One of the fundamental aspects of structural behavior is bond development, since bond is the key for the “co-operation” of reinforcing bars and concrete. An adequate level of bond is required between reinforcement and concrete to transmit forces from one to another (Pilakoutas et al 1997).

Bond of steel reinforcement to concrete has been studied extensively in the last 40 years and a huge amount of experimental and analytical work has been published on this subject (CEB Bulletin 151, 1982, *fib* bulletin 10, 2000). However, the design formulae of the most current design codes of practice do not incorporate any provisions for the use of alternative reinforcing materials other than steel. In the best cases, some provisions for epoxy-coated bars are considered. The introduction of FRP reinforcing bars has created the necessity for the development of design specifications that will allow engineers to use these materials as reinforcement in concrete structures.

In order to overcome this problem, engineers and researchers round the world are currently intensifying their efforts to understand how these new materials actually interact with concrete, in order to be able to contribute towards the formulation of design codes of practice. A part of this research effort was the EUROCRETE project (Clarke and Waldron, 1996). EUROCRETE was a 4-year research project, which investigated the use of non-ferrous (FRP) reinforcement in concrete structures. The EUROCRETE project led to the development of a new durable FRP bar, which is now commercially available in the market and the production of design guidelines (IStructE, 1999)

Two major experimental series of tests were conducted under the EUROCRETE project to investigate the bond behavior of FRP reinforcement in concrete structures (Achillides, 1998). In the first series, more than 100 specimens were tested in direct pullout whereas in the second, the bond splitting behavior of FRP reinforcing bars was examined in nine concrete beams tested under four-point bending. In this paper the main emphasis is placed on the pullout tests, whereas the beam tests will be presented in detail in a following publication. The work described in this

paper is also part of the work of the European Union Funded research network CONFIBRECRETE, which aims the development of design guidelines for FRP reinforced concrete structures in association with task group 9.3 of the International Federation of Concrete (fib).

PULLOUT TESTING

Pullout tests are used commonly in the assessment of bond performance of steel reinforcing bars in concrete. Although the stress conditions developed in the concrete specimen during pullout tests are rarely encountered in practice and the bond values developed under those tests differ substantially from those developed in reinforced concrete elements for most practical conditions, pullout tests are widely adopted. For this reason they offer an economical and simple solution for the evaluation of bond performance of reinforcing bars and represent in a simple manner the concept of anchoring a bar (Cairns and Abdullah, 1995). However, it should be stressed that good bond in well confined pullout tests does not mean that good bond can be achieved in a concrete member where the cover resistance against splitting determines the ultimate failure load.

The main aim of bond tests is to obtain the bond-slip relationship at the loaded and free ends of FRP bars subjected to a pullout load. A careful evaluation of the pullout arrangements used for steel bars by previous researchers, was conducted in order to find the most appropriate set-up for the experimental purposes. The investigation resulted in two options of pullout tests: the Losberg

(1963) and RILEM/CEB/FIP (1978) arrangements shown in figure 1, both of which are used commonly for the evaluation of bond of steel bars.

However, the authors were initially concerned about the accuracy of the measurements of slip at the end of the bar obtained by the RILEM test, since the embedment length of the bar is at the very end of the cube. In this case, any deformation at the end of the concrete due to the pullout load would be recorded as bar slip although it is not actually slip. For this reason a modified version of Lowberg's test was adopted. However, at a later stage of the testing series some specimens were prepared having the bar-concrete contact area at the end of the bar, similar to the RILEM arrangement, in order to investigate differences in the bond development by the two arrangements.

The selection of primary variables for this study was based on existing experience of bond behavior of steel bars in concrete. The most important factors examined were; the type of bar fiber, the concrete strength, the diameter of bar, the shape of bar, the type of bar surface characteristics, the embedment length and the effect of embedment length location in the concrete cube.

These factors were expected to have a different influence on the bond behavior of FRP bars since FRP materials are strongly anisotropic and have different mechanical properties than steel bars. A proper evaluation of the influence of these factors on bond development is crucial to the understanding of how actually these materials "co-operate" with concrete in structural members and for the estimation of adequate anchorage lengths.

SPECIMEN PREPARATION AND MATERIAL PROPERTIES

Prior to casting, the FRP bars were properly marked so that the embedment length would lie in the middle of the concrete cube. The embedment lengths were designed as multiples of the bar diameter to facilitate comparisons among different diameter bars. The two ends of the bar in the concrete cube were wrapped with several layers of cling film in order to form non-contact (debonded) areas between bar and concrete. The bars were then positioned vertical in 150 mm cube moulds where concrete was cast around the bar.

Material Properties

Concrete: More than ten castings were made during the period of the research study. The concrete mixes had average compressive strengths in the range of 15.5 to 49.5 MPa. The concrete cube (150 mm side) compressive strength values for each batch of pullout tests are presented in Tables 1 to 3 in appendix A, together with the experimental results for each test.

FRP materials: The FRP bars tested were pultruded during the development stages of the EUROCRETE bar, using a vinyl ester hybrid resin. Up to 70% volume fraction was achieved during the pultrusion process. Three kinds of fibers were initially tried for the manufacture of four types of reinforcing bars: Carbon, E-Glass, Aramid and Hybrid (Carbon + Glass together). However, the bulk of the testing was done using bars with the two first types of fiber, which seemed more promising for the purposes of the project. The surface deformations are created by the addition of a peel-ply on the surface of the bar during pultrusion, which is removed after the

settlement and curing of the resin. This procedure created a rough external surface on the bar with an average peak height of 0.75 mm (see figure 2).

The bars that were tested in this experimental series had different types of cross-sectional areas, sizes and surface deformation textures as shown in Table 1. The Young's modulus of elasticity of the EUROCRETE FRP bars was evaluated by direct tension tests and the average values obtained are presented in Table 2 (Duranovic et al, 1995). The supplier's characteristic tensile strength of the various bars is also given in the table.

Experimental procedure

The pullout test schematic arrangement adopted is shown in Figure 3. The concrete cube with the embedded FRP bar was placed in a specially made steel frame that was positioned in the testing machine. The rig consisted of two steel plates 25 mm thick, which were connected at the four edges with four 20 mm diameter rods. The top plate had a 30 mm diameter hole in its center allowing the FRP bar to run through. On this plate there were also another three additional holes in a triangular arrangement round the main hole, which allowed three LVDTs (linear voltage displacement transducers), located at the loaded end of the specimen, to touch the top surface of the concrete cube. A fourth LVDT was attached on a small aluminum frame that was glued to the bottom surface of the concrete cube to measure the slip at the free (unloaded) end of the bar. The bottom end of the rig was secured in the jaws of the testing machine, which provided the reaction to the pullout load resisted by the specimen.

Between the concrete block and the bearing steel plate, a 5mm thick wooden plate was introduced to secure the contact between the top surface of the concrete block and the steel bearing plate. This was necessary since small irregularities at the top surface of the cube might introduce accidental bending on the bar during loading or movements due to local crushing.

The test specimen was positioned in a universal testing machine, which applied to the specimen direct tension in a deflection-control mode (at a maximum rate of about 0.1 kN/sec). The test was only stopped when slip at the loaded end of the bar was greater than 8 mm.

Analysis of measurements

The measurements obtained from the experimental results were used to produce the bond-slip curves for each specimen. The average displacement measured of the three LVDTs does not represent only the bar slip, but also the rebar extension above the embedment length. Hence, the elongation of the length of the bar, l_a, from the transducer support point to the level of the bonded bar (see Figure 3) is subtracted from the measurements. The bond-slip displacement at the unloaded end of the bar is obtained directly from the slip measurement of the bottom LVDT.

The average bond stress, τ_{av}, at any stage during loading is the recorded pullout load on the bar, F, divided by the nominal surface area of the embedment length, L, of the bar. For a circular bar diameter d, this is given by the relationship:

$$\tau_{av} = F / (\pi\, d\, L) \qquad (1)$$

The maximum average bond value, τ^*, is obtained by Eq. (1) when the pullout load reaches its maximum value (F_{max}) during the test.

EXPERIMENTAL RESULTS

The results of 131 cube tests are used to evaluate the bond behavior of FRP reinforcing bars to concrete. A summary of the experimental results is presented in Tables 1 to 3 of appendix A. The general coding notation applied for the rough surface bars embedded in concrete cubes is as follows:

1. The first number of the code indicates the concrete cube compressive strength in MPa
2. The first letter denotes the kind of reinforcing bar used in the test (G for GFRP bar, C for CFRP, A for AFRP and H for Hybrid)
3. The next letter denotes the type of the bar cross section (r for round and s for square)
4. The second number indicates the ratio of embedment length to the bar diameter (applies only in round bars)
5. The last letter denotes the size of the bar diameter (D for 13.5 mm, d for 8 or 8.5 mm and *d* for 10.5 mm).

For example, 45Gr8D designates a 13.5 mm GFRP round bar, cast in concrete with compressive strength 45 MPa, having embedment length equal to 8 times the bar diameter.

Bond stress versus Slip curve

Fig. 4 shows typical plots of bond stress versus slip of GFRP and CFRP reinforcing bars. As seen from the curves, the loaded end slips almost at the beginning of loading as soon as the chemical adhesion between bar and concrete breaks. According to CEB Bulletin 151 (1982), in the case of steel bars the bond resistance offered by adhesion is assumed to be rather small around 0.5-1.5 MPa. However, the Bulletin does not state whether this value is derived from experimental data or it is a theoretical estimation.

Since the required level and accuracy of slip measurements for this purpose is not determined anywhere in the literature, it is difficult to determine accurately the adhesion between FRP bars and concrete. In addition, high accuracy in slip measurements can hardly be expected at the beginning of the tests since many factors (such as local bending) influence the accuracy of the loaded end slip measurements at that stage.

Considering the above, it was decided to estimate the level at which the chemical adhesion of an FRP bar and the concrete breaks by visual examination of the bond-slip curves. This was accomplished by finding the point, at the initial loading stage, at which the slope of the average bond stress versus the loaded end slip curve decreases significantly. The experimental results show that the adhesive bond strength seems to depend only on the bar diameter, whereas it appears to be independent of the type of bar fibres and the concrete used in the specimens. Figure 5 shows the average value of adhesion measured in the experiments where smaller diameter bars develop greater adhesion with the surrounding concrete than larger bars.

Another important observation from the tests is that the unloaded end slip remains practically zero until the bond stress reaches quite high levels compared with the ultimate bond strength.

The results showed that the average ratio of the bond stress when the unloaded end started to slip to the maximum bond strength is around 80 % for both G and CFRP bars (Achillides, 1998). Although the ratio was initially assumed to depend on the elastic modulus of the bar, the results suggested no clear relationship between the two quantities.

The initial slope of the loaded end bond-slip curve for CFRP bars is stiffer than that of GFRP bars and this is clearly related to the difference in the elastic moduli of the two bars. However, apart from the elastic modulus, the initial slope is influenced by other parameters as will be examined later.

The residual (post-maximum) bond strength value appears to be more than 60% of the peak bond value in most of the specimens. This seemed to be an important attribute of FRP bars since the residual stress of deformed steel bars under similar tests was only 20 to 40% of the maximum value. However, the above value may be unrealistic as will be explained after the discussion on the mode of bond failure.

Bond failure mode of FRP bars

In the described experiments, all FRP bars failed in the designed pull-through mode of bond failure. The concrete cubes provided adequate confinement to the bars to enable them to reach their maximum bond strength. No signs of splitting cracks appeared on the cube specimens since the diameter and embedment length of the bars was relatively small to the dimensions of the cube specimens.

However, by comparing the mode of failure of FRP bars to that of steel deformed bars under similar experimental conditions, an important difference was observed. When sufficient confinement is provided to a deformed steel bar during pullout, shear cracks develop between the bar ribs and the surrounding concrete before the bar fails in a pull-through mode. When this kind of failure happens, the bond strength of the bar depends mainly on the strength of the surrounding concrete. Nevertheless, the bond strength of FRP bars does not appear to be controlled by the concrete strength.

In the case of FRP bars and for concrete strengths greater than 30 MPa, bond failure occurs partly in the surface of the bar, and partly in the concrete, by peeling part of the surface layer of the bar. Fig. 6 shows a characteristic GFRP specimen sample after the test. The cube was split after the test, for a closer investigation of the actual mode of bond failure. It is obvious from this figure that a white powder (consisting of crushed resin and chopped glass fiber) is attached on the concrete cube at the location of the embedment length. In addition, the bar was scratched and tiny fibers could be seen on the surface of the bar by the naked eye.

The failure appears to develop at a critical interface between successive layers of fibers as shown schematically in Fig. 7. The shear strength between fibers and resin seems to control the bond capacity of FRP bars in both cases. The height of the failure interface from the bar axis is assumed to depend on the relative value of shear strength between fibers and resin and the concrete shear strength. In the current experiments, the height of the failure interface of GFRP bars is assumed to be lower than that of CFRP bars, since the GFRP bar surface was more extensively damaged.

For lower strength concrete (around 15 MPa) FRP bars failed in a different mode, more similar to deformed steel bars. The concrete crushes in front of the deformations of the bar and the bond strength appears to be controlled mainly by the shear strength of the concrete. The bond strength values developed in this case were significantly lower than the ones developed in higher strength concrete.

Residual bond strength of FRP bars

As a result of the type of bond failure of FRP bars in higher strength concrete (f_{cu} > 30 MPa), it is believed that the recorded residual bond stress, shown in Fig. 4, does not necessarily represent the real value of frictional stress developed at the failure interface. This is due to the fact that when the damaged part of the bar is slipping out of the cube during pullout, the undamaged part that follows enters the embedment length zone, as shown in Fig. 8, and adds additional resistance to the pullout load. This action enhances the recorded bond strength value that represents, apart from the frictional stress, the additional resistance produced by the wedging action of the undamaged bar.

The above phenomenon is unimportant for steel bars since the bond failure happens in the surrounding concrete. As a result, the unbonded part of the bar which enters the embedment length zone does not contribute significantly to the bond resistance of the bar since the bond failure interface is approximately at the height of the tips of bar deformations.

To quantify the value of the residual bond stress resulting solely due to frictional action, an additional series of experiments was conducted where some of the specimens had the

embedment length at the very end of the cube as shown in Fig. 1 (similar to the RILEM pullout test). The test arrangement and instrumentation used were similar to the one used during the experimental series presented above.

The results of the additional series of tests are presented at the second half of Table 3 in appendix A. Analysis of the results showed that the residual bond stress was much lower in this case with the embedment length at the end of the specimen (Achillides, 1998). The difference was more important in GFRP than in CFRP bars (Fig. 9) and this can be attributed to differences in the depths of the bond failure interface (see Fig. 7).

Nevertheless, the position of the embedment length in the concrete cube does not seem to influence the maximum bond stress developed or the initial bond stiffness of round FRP bars. This can be explained by the fact that the unloaded end slip values recorded up to the maximum pullout load were less than 1 mm in all the specimens and the wedging effect could not be significantly activated in such a short distance. On the contrary, in some cases of square bars a small difference in the maximum recorded bond values was observed for the two positions of embedment length and this will be discussed in more detail later.

FACTORS THAT INFLUENCE THE BOND BEHAVIOR OF FRP BARS

Important factors that influence the bond behavior of FRP bars are examined in the following. A proper evaluation of the level of influence of these factors on the bond development will be helpful to the formulation of equations for adequate anchorage lengths for FRP reinforcement.

Type of bar fiber

The maximum average bond stress (τ^*) developed for GFRP and CFRP bars is shown in figure 10, versus the embedment length (L). The examined specimens were 8 and 8.5 mm diameter round bars of rough surface. By using linear regression, the best-fit line passing through all data points was obtained, even though it is not intended to show that a linear relationship exists between τ^* and embedment length. Over the small range of embedment lengths (2 to 10 times the diameter), linear regression is used only for comparison purposes

From Fig. 10 it can be seen that both Carbon and Glass FRP bars exhibited similar bond behavior. Their maximum average bond stress at the embedment length of 8 diameters (L = 64 mm) was 11.9 and 12.0 MPa, respectively. By comparison, deformed steel bars, having the same diameter and embedment length, developed τ^* equal to 16.5 MPa (for concrete strength 39 MPa). From the above figures, it can be deduced that GFRP and CFRP bars developed about 72% of steel's bond strength, which is quite remarkable considering the different nature of their surface and type of bond failure. However, it has to be noted that the above percentage is not representative for the whole range of values of concrete strength since the influence of the concrete strength on the bond strength of FRP and steel bars is not the same. For lower concrete

strengths (around 30 MPa) the bond strength of steel bars will decrease whereas the FRP bar bond strength will remain practically the same.

As can be seen from the tables in the appendix, Aramid and Hybrid FRP bars developed around 85% and 90% of the Glass and Carbon FRP bond strength, respectively, which is also quite satisfactory. It has to be noted that the development of the Aramid bar during the Eurocrete project was not completed and it is not expected that well manufactured AFRP bars will behave differently from Glass or Carbon FRP.

The above experimental results appear to be in agreement with results published by other researchers (Malvar, 1995, Larralde and Silva-Rodriqez, 1993, Chaallal and Benmokrane, 1993 and Nanni, Al-Zaharani, Al-Dulaijen, Bakis and Boothby, 1995, Tepfers R. and Karlsson M., 1997) despite the fact that different types of FRP rods were used. It is also worth noting that the bond strength of epoxy-coated bars, which are mainly used as anti-corrosive reinforcement, varies from 67-95% of that of deformed steel bars (Chaallal and Benmokrane, 1993), which is comparable to the bond strength of FRP bars.

Embedment length

An increase in embedment length is shown in Fig. 11 to decrease the maximum average developed bond stress value (τ^*). The same effect is also reported for steel bars and is thought to be a result of the non-linear distribution of bond stress on the bar. The embedment length also has significant influence on the initial bond stiffness of FRP bars. The rate of increase of bond

stress is greater for smaller than for larger embedment lengths. This is again assumed to be due to the non-linear distribution of bond stresses on the bar.

Concrete strength

Results from this study showed that the strength of the concrete affects the actual mode of bond failure of the bar during pullout. Fig. 12 shows τ^* versus concrete strengths for an embedment length of 6d. For concrete with compressive strength greater than 30 MPa, the bond failure interface happens at the surface of a FRP bar. Consequently, in such concrete, the bond strength of FRP bars does not depend much on the value of concrete strength. However, for lower concrete strengths (around 15 MPa) the bond failure mode changes. In this case the failure interface takes place in the concrete matrix and the bond behavior of the bar is directly related to the concrete strength

Bar diameter

Larger diameter bars are shown in the tables in the Appendix to develop less average bond strength than smaller diameter bars and it was seen earlier in this paper that they loose their adhesive bond earlier. Three factors may be responsible for their lower bond strength: embedment length, Poisson effect and shear lag.

Embedment length: Larger diameter bars require longer embedment lengths to develop the same normal bond stress. As shown earlier, larger embedment lengths reduce the average bond strength.

Poisson effect: The Poisson effect can lead to the slight reduction in bar diameter as a result of the longitudinal stress. This bar reduction increases with bar size, which can lead to reduced frictional/mechanical locking stresses.

Shear lag: The shear stiffness of FRP bars depends mainly on the shear stiffness of the resin and the shear strength at the resin-fiber interface. When an FRP bar is pulled in tension through the surface, there can be some differential movement between the core and the surface fibers, which results in a non-uniform distribution of normal stresses through the cross section of the bar. A diagrammatic distribution of these stresses is shown in Fig. 13. This "shear lag" effect leads to higher surface normal stresses, σ_{Max} which "govern" the bond strength of the bar, whereas the calculated average stress, σ_{Ave} is lower. The difference in these stresses is greater in large diameter bars and is expected to reduce the estimated average bond strength.

Cross sectional shape of the bar

Square (8 x 8 mm) and round (8 or 8.5 mm diameter) cross sections were examined. By comparing the results for bars with the same embedment lengths, the square bars appeared to develop superior bond strength values than round bars by up to 25% since the wedging effect (reported previously) is more important in the case of square bars due to their sharp edges. A closer examination of square bar specimens after pullout supports the above assumption since the bar edges appeared to deteriorate more than the rest of the bar surface.

Surface deformations

Preliminary research showed that the presence of deformations on the surface of FRP bars play a significant role on their bond behavior since smooth bars appeared to develop only 10-20% of the bond stress of the deformed bars. Similarly to steel bars, the bond strength of FRP bars is assumed to depend mainly on the mechanical interlock of the surface deformations and the concrete matrix, rather than on the chemical adhesion of the two materials.

In order to investigate the influence of the height of deformations on the bond strength of FRP bars, GFRP bars having different bar deformation heights were tested. Table 2 of appendix A shows the experimental results, for two types of 10.5 mm GFRP round bars (G24, G30) having smaller surface deformations (0.20 and 0.25 mm, respectively) than the standard 8.5 mm deformed bars used in this series (deformation average height 0.75 mm). A comparison of the average bond values developed from these bars is given in Fig. 14.

It is clear from the figure that G24 and G30 FRP bars did not perform as well as the standard deformed EUROCRETE GFRP bar. It can be concluded that FRP bars must necessarily have a minimum height of deformations to develop satisfactory bond behavior to concrete. The deformation height was not studied extensively in this research project since only a limited range of FRP bars was available for testing. However, the above results appear to agree with observations by Malvar (1995), who suggests that surface deformations of about 5.4% of the bar diameter are sufficient to provide adequate bond behavior to concrete.

CONCLUSIONS

– All the specimens in the experimental series of pullout tests failed in a pull-through mode of failure since the concrete cube provided adequate confinement to the bars to enable them to reach their maximum bond strength. The mode of bond failure of FRP bars in most cases differs from the mode of bond failure of steel deformed bars. For concrete strengths greater than 30 MPa, failure occurs partly on the surface of the bar, and not just in the concrete as in the case of steel bars, by peeling away part of the surface layer of the bar. Consequently, the bond strength of FRP bars is not controlled as much by the concrete strength, but appears to be influenced by the interlaminar shear strength just below the resin rich surface layer of the bar. For concrete strengths less than 15 MPa, the concrete is crushed in front of the bar deformations and the bond strength is controlled mainly by the shear strength of concrete.

– Chemical adhesion in the FRP bars and free end slip appear to be correlated and they happen when the bond stress is around 80% of the bond strength. This is much higher that expected for conventional steel reinforcement.

– No significant difference was found between the bond strengths developed by GFRP and CFRP bars. Aramid and Hybrid ‘development’ bars showed slightly lower bond strengths.

– In the pull-out test, an increase in the embedment length is accompanied by a decrease in bond strength.

– Smaller diameter bars develop higher bond strength than larger diameter bars, whilst square bars develop up to 25% higher bond strength than round bars. The “wedging effect” due to the sharp edges seems to be responsible for this difference.

– A minimum average height of deformations of 0.75 mm was found necessary to develop satisfactory bond behavior to concrete.

ACKNOWLEDGEMENT: The authors would like to acknowledge the technical and financial assistance offered by the Centre for Cement and Concrete of the University of Sheffield, the EUROCRETE project and the EU TMR CONFIBRECRETE research network.

REFERENCES

Achillides Z. (1998), “Bond behaviour of FRP bars in concrete”, PhD Thesis, Centre for Cement and Concrete, Dept. of Civil and Structural Engineering, The University of Sheffield, UK, 355 pp

Achillides Z., Pilakoutas K. and Waldron P. (1997 a), "Modelling of FRP rebar bond behaviour", 3rd International Symposium on Non-Metallic (FRP) Reinforcement for Concrete Structures, 14-16, Sapporo, Japan, 423-430

Achillides Z., Pilakoutas K. and Waldron P. (1997 b), "Bond behaviour of FRP bars to concrete", Procs 3rd Int. Symp. on Non-Metallic (FRP) Reinforcement for Concrete Structures, Sapporo, Japan, Japan Concrete Society, 341-348

Cairns J. and Abdullah R. (1995), “An evaluation of bond pullout tests and their relevance to structural performance”, J. The Structural Engineer, 73(11), 179-185

CEB *Bulletin 151* (1982), 'Bond action and bond behaviour of reinforcement', State-of-the-Art Report, Comitee Euro-international du Beton Bulletin 151

Chaallal O., Benmokrane B. (1993), "Pullout and bond of glass-fibre rods embedded in concrete and cement grout", J. Materials and Structures, 26, 167-175

Clarke J. and Waldron P. (1996), "The reinforcement of concrete structures with advanced composites", J. The Structural Engineer, 74(3), 283-288

Duranovic N., Pilakoutas K., Waldron P. (1995), "General Testing Arrangement on R.C. Beams", Report No. CCC/94/0017A, Centre for Cement and Concrete, Dept. of Civil and Structural Eng., University of Sheffield, UK

fib bulletin *10* (2000) "Bond of non-metallic reinforcement", Chapter 7 in "Bond of Reinforcement in Concrete", State of the art report prepared by Task Group Bond Models, International Federation for Structural Concrete, Switzerland, 315-394

Head P.R. (1996), "Advanced composites in civil engineering - a critical overview at this high interest, low use stage of development", Advanced Composite materials in bridges and structures, 2nd Inter. Conf., Montreal, Quebec, Canada, 3-16

IstructE (1999), 'Interim Guidance on the Design of Reinforced Concrete Structures Using Fibre Composite Reinforcement', The Institution of Structural Engineers, London, UK

Larralde J. Silva-Rodriqez R. (1993),"Bond and slip of FRP repairs in concrete", J of Materials in Civil Eng., 5(1), 30-39

Losberg A. (1963), "Force transfer and stress distribution at anchorage and curtailment of reinforcement", Chalmers University of Technology, Department of Building Technology, No 608, Goteborg 1963, p.49

Malvar J. L. (1995), "Tensile and Bond Properties of GFRP Reinforcing Bars", J. ACI Materials, 92(3), 276-285

Nanni A., Al-Zaharani M., Al-Dulaijen S., Bakis S. and Boothby T. (1995), "Bond of FRP reinforcement to concrete - Experimental results", Non-Metallic (FRP) Reinforcement for Concrete Structures, ed. L. Taerwe, 137-145

Pilakoutas K, Achillides Z and Waldron P (1997), "Non-Ferrous reinforcement in concrete structures", in Innovation in Composite Materials and Structures, Eds M.B. Leeming & B.H.V. Topping, Civil-Comp Ltd, Edinburgh, 47-58

Pilakoutas K. (2000), 'Composites in Concrete Construction', in "Failure Analysis of Industrial Composite Materials", Gdoutos A., Pilakoutas K. and. Rodopoulos C. (Eds), McGraw-Hill Professional Engineering, 449-497

RILEM/CEB/FIP (1978) *Recommendation RC6*, "Bond test for reinforcing steel 2. Pullout test", RILEM/CEB/FIP

Rostasy F.S (1996), “FRP: The European Perspective”, Fiber Composites in Infrastructure”, 1st Inter. Conf. in Infrastructure, ed. Saadatmanesh and Eshani, Arizona, 12-20

Tepfers R. and Karlsson M. (1997), “Pull-out and tensile reinforcement splice tests using FRP C-Bars”, Proceedings of the 3rd International Symposium on Non-Metallic (FRP) Reinforcement for Concrete Structures: Non-Metallic (FRP) Reinforcement for Concrete Structures, JCI, Vol. 2, Sapporo, Japan, pp 357-364

LIST OF TABLES

Table 1—Types of bars used in pullout tests

Type of Bar	Surface texture	Dimensions of cross-section (mm)	Cross-sectional area (mm^2)
GFRP round	Rough	13.5	143.13
GFRP round	Rough	8.5	56.27
GFRP round	Medium rough h_{def} < 0.25 mm	10.5	86.59
GFRP square	Rough	8.5 x 8.5	72.25
GFRP round	Smooth	16	201.06
Carbon round	Rough	13.5	143.13
Carbon round	Rough	8	50.26
Carbon ring	$Rough_{out}$, - $smooth_{in}$	d_{out} = 21-d_{in}= 10	267.82
Carbon square	Rough	8.5 x 8.5	72.25
Aramid round	Rough	13.5	143.13
Aramid round	Rough	8.5	56.27
Aramid square	Rough	8.5 x 8.5	72.25
Hybrid round	Rough	13.5	143.13

Table 2—Mechanical properties of FRP bars

	GFRP	CFRP	AFRP	HFRP
Young Modulus (MPa)	45000	115000	67000	51000
Tensile strength (MPa)	>1000	>1500	>1500	>1000

APPENDIX A

Table 1	D mm	L mm	F_{max} kN	δ_1 mm	δ_2 mm	τ^* MPa	f_{cu} MPa
37Gr2DI	13.5	27	14.5	~	~	12.7	37
37Gr2DII	13.5	27	16.7	~	~	14.6	37
37Gr4DI	13.5	54	31.7	~	~	13.8	37
37Gr4DII	13.5	54	27.3	~	~	11.9	37
49Gr6DI	13.5	81	43.0	~	~	12.5	49
49Gr6DII	13.5	81	44.7	~	~	13.0	49
46Gr6DI	13.5	81	43.1	~	~	12.6	46
46Gr6DII	13.5	81	45.3	~	~	13.2	46
46Gr6DIII	13.5	81	26.9	~	~	7.8	46
46Gr6DIV	13.5	81	48.2	~	~	14.0	46
49Gr8DI	13.5	108	51.2	~	~	11.2	49
49Gr8DII	13.5	108	45.3	~	~	9.9	49
46Gr10DI	13.5	135	48.4	~	~	8.5	46
46Gr10DII	13.5	135	53.5	~	~	9.3	46
30Cr2DI	13.5	30	13.5	~	~	10.6	30
30Cr3DI	13.5	45	21.2	~	~	11.1	30
30Cr4.5DI	13.5	60	27.5	~	~	10.8	30
30Cr5.5DI	13.5	75	23.4	~	~	7.4	30
46Cr6DI	13.5	81	40.4	~	~	11.8	46
46Cr6DII	13.5	81	50.1	~	~	14.6	46
45Gr2D	13.5	27	13.4	0.58	0.57	11.7	45
45Gr4D	13.5	54	23.0	0.66	0.47	10.0	45
45Gr6D	13.5	81	41.0	0.91	0.48	11.9	45
45Gr8D	13.5	108	40.5	0.96	0.21	8.9	45
45Gr10D	13.5	135	51.9	1.03	0.32	9.1	45
45Cr2D	13.5	27	15.1	0.43	~	13.2	45
45Cr4D	13.5	54	32.1	0.44	0.34	14.0	45
45Cr6D	13.5	81	30.1	0.44	0.25	8.8	45
45Cr8D	13.5	108	44.8	0.55	0.32	9.8	45
45Cr10D	13.5	135	44.2	0.53	0.19	7.7	45
45Ar6D	13.5	81	34.8	0.42	0.33	10.1	45
45Hr6D	13.5	81	37.3	0.72	0.23	10.9	45
45Gr10d	8.5	81	16.5	0.66	0.40	8.1	45
45Cr10d	8	81	15.3	0.49	0.25	7.5	45
45Cc	21	81	46.1	~	~	8.6	45
45Gsm	16	81	4.9	0.65	~	1.2	45
45Hsm	8	81	2.6	0.19	0.02	1.3	45
45Gs	8x8	81	24.5	0.99	0.41	8.9	45
45Cs	8x8	81	25.0	0.57	0.32	9.0	45
45As	8x8	81	14.8	~	~	5.4	45

Notation:

D = Diameter of bar / dimensions of bar's cross section

L = Embedment length

F_{max} = Maximum pull-out load

δ_1 = Loaded end slip at F_{max}

δ_2 = Unloaded end slip at F_{max}

τ^* = Maximum average bond stress

Table 2	D mm	L mm	F_{max} kN	δ_1 mm	δ_2 mm	τ^* MPa	f_{cu} MPa
15Gr2D	13.5	27	3.2	0.79	0.65	2.8	15
15Gr4D	13.5	54	7.1	0.44	0.42	3.1	15
15Gr6D	13.5	81	6.7	0.80	0.70	1.9	15
15Gr8D	13.5	108	11.5	0.67	0.47	2.5	15
15Gr10D	13.5	135	14.8	0.81	0.42	2.6	15
15Cr2D	13.5	27	4.2	0.44	0.43	3.7	15
15Cr4D	13.5	54	8.0	0.48	~	3.5	15
15Cr6D	13.5	81	10.8	0.30	0.16	3.1	15
15Cr8D	13.5	108	13.0	0.40	0.29	2.8	15
15Cr10D	13.5	135	12.7	0.49	0.41	2.2	15
15Ar6D	13.5	81	4.2	1.17	1.11	1.2	15
15Hr6D	13.5	81	7.6	0.65	0.53	2.2	15
15Gr10d	8.5	81	4.8	0.70	0.51	2.3	15
15Cr10d	8.0	81	4.4	0.43	0.28	2.2	15
15Ar10d	8.0	81	4.9	0.37	0.23	2.4	15
15Cc	21.0	81	15.6	0.74	0.62	2.9	15
15Gsm	16.0	81	0.3	0.37	0.36	0.1	15
15Hsm	8.0	81	1.4	0.09	~	0.7	15
15Gs	8x8	81	8.7	0.42	0.14	3.1	15
15Cs	8x8	81	5.6	0.48	~	2.0	15
15As	8x8	81	7.4	0.24	0.00	2.7	15
41Gr6dI	8.5	48	15.6	1.27	1.16	12.2	41
41Gr6dII	8.5	48	11.9	1.01	0.80	9.3	41
41Gr8dI	8.5	64	21.9	1.07	0.75	12.8	41
41Gr8dII	8.5	64	24.8	1.07	0.71	14.5	41
41Gr10dI	8.5	80	25.6	1.31	0.65	12.0	41
41Gr10dII	8.5	80	28.8	-	-	13.5	41
41Cr6dI	8	48	16.9	0.43	0.37	14.0	41
41Cr6dII	8	48	15.4	0.46	0.31	12.7	41
41Cr8dI	8	64	22.1	0.59	0.37	13.7	41
41Cr8dII	8	64	22.2	0.51	0.02	13.8	41
41Cr10dI	8	80	25.7	0.73	0.41	12.8	41
41Cr10dII	8	80	28.7	0.53	0.34	14.3	41
41G24/6*d*I	10.5	60	10.4	0.24	0.96	5.3	41
41G24/6*d*II	10.5	60	8.0	0.23	0.02	4.0	41
41G24/8*d*I	10.5	80	11.0	0.39	0.04	4.2	41
41G24/8*d*II	10.5	80	13.3	0.51	0.16	5.0	41
41G24/10*d*I	10.5	100	12.4	0.37	0.08	3.8	41
41G24/10*d*II	10.5	100	18.7	0.55	0.13	5.7	41
41G30/6*d*I	10.5	60	9.2	0.27	0.04	4.7	41
41G30/6*d*II	10.5	60	9.1	0.26	0.06	4.6	41
41G30/8*d*I	10.5	80	18.3	0.60	0.18	6.9	41
41G30/8*d*II	10.5	80	10.6	0.37	0.10	4.0	41
41G30/10*d*I	10.5	100	20.2	0.51	0.05	6.1	41
41G30/10*d*II	10.5	100	22.0	-	-	6.7	41

Additional Notation

Cc = CFRP bar with ring cross section (r_{out}=21mm, r_{in}=10mm)

Gsm = GFRP smooth surface bar

Hsm = Hybrid smooth surface bar

G24= GFRP round bar with different type of surface deformations (24 rovings)

G36= GFRP round bar with different type of surface deformations (36 rovings)

Table 3	D mm	L mm	F_{max} kN	δ_1 mm	δ_2 mm	τ^* MPa	f_{cu} MPa
39GSAI	8x8	64	32.1	0.88	0.67	15.7	39
39GSAII	8x8	64	32.5	0.70	0.19	15.9	39
39GSAIII	8x8	64	31.9	0.87	0.16	15.6	39
39Gr8dI	8.5	64	20.1	0.92	0.63	11.7	39
39Gr8dII	8.5	64	20.3	0.95	0.65	11.9	39
39Gr8dIII	8.5	64	16.6	0.63	0.34	9.7	39
39Cr8dI	8	64	19.4	0.57	0.45	12.0	39
39Cr8dII	8	64	15.7	0.64	0.07	9.8	39
39Cr8dIII	8	64	16.9	0.57	0.50	10.5	39
39GSDI	8x8	64	25.5	0.96	0.37	12.5	39
39GSDII	8x8	64	31.5	1.00	0.42	15.4	39
39GSDIII	8x8	64	22.5	0.95	0.44	11.0	39
39CSI	8x8	64	31.4	0.45	0.20	15.3	39
39CSII	8x8	64	30.3	0.50	0.00	14.8	39
39CSIII	8x8	64	27.8	0.40	0.00	13.6	39
39GsI	8x8	64	26.6	0.84	0.64	13.0	39
39GsII	8x8	64	26.0	0.94	0.70	12.7	39
39CsI	8x8	64	24.6	0.57	-	12.0	39
39CsII	8x8	64	21.9	0.60	0.39	10.7	39
39GSTI	10x10	81	7.5	6.80	6.20	2.4	39
39GSTII	10x10	81	11.0	6.65	5.10	3.4	39
39Ar8dI	8	64	18.0	0.55	0.24	11.2	39
39Ar8dII	8	64	15.4	0.49	0.22	9.6	39
36GSAI	8x8	64end	29.2	0.92	0.07	14.3	36
36GSAII	8x8	64end	27.3	0.73	0.35	13.4	36
36GSAIII	8x8	32end	13.5	0.18	0.28	13.3	36
36GSAIV	8x8	32end	17.4	0.54	0.37	17.2	36
36Gr4dI	8.5	32end	10.1	0.80	0.75	11.8	36
36Gr4dII	8.5	32end	11.8	0.51	0.40	13.8	36
36Gr4dIII	8.5	32mid	10.2	0.50	0.31	11.9	36
36Gr4dIV	8.5	32mid	10.1	0.96	0.94	11.8	36
36Cr4dI	8	32end	8.7	0.57	0.62	10.8	36
36Cr4dII	8	32end	10.1	0.72	0.54	12.6	36
36Cr4dIII	8	32mid	10.2	0.44	0.37	12.7	36
36Cr4dIV	8	32mid	8.6	0.33	0.33	10.7	36
36CSI	8x8	64end	27.2	0.50	0.36	13.3	36
36CSII	8x8	64end	27.2	0.27	-	13.3	36
36GsI	8x8	64end	18.8	1.13	0.49	9.3	36
36GsII	8x8	64end	22.1	0.83	0.76	10.9	36
36CsI	8x8	32end	10.5	0.43	0.39	10.4	36
36CsII	8x8	32end	14.0	0.60	0.38	13.9	36
36StI	8	64end	26.7	0.88	0.87	16.6	36
36StII	8	64end	26.5	0.29	0.78	16.5	36

Additional Notation

GSA = GFRP square (different kind bar surface deformations and resin)

CS = CFRP square (different kind bar surface deformations and resin)

GSD = GFRP square (different kind of resin)

GST = GFRP square smooth bar with twisted shape

St = High strength steel deformed bar

LIST OF FIGURE CAPTIONS

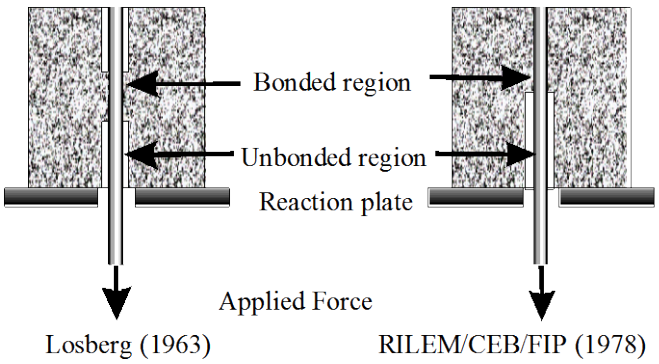

Fig. 1—Typical pullout tests

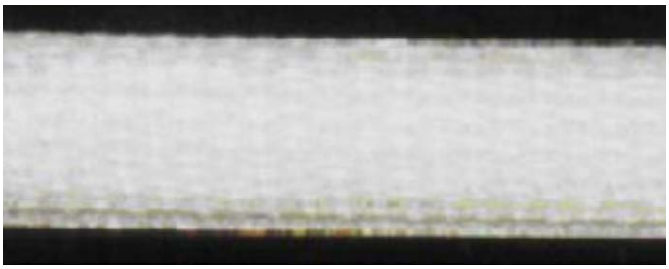

Fig. 2— EUROCRETE GFRP bar

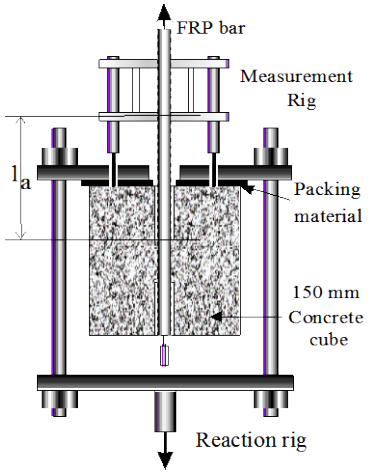

Fig. 3—The pullout test arrangement

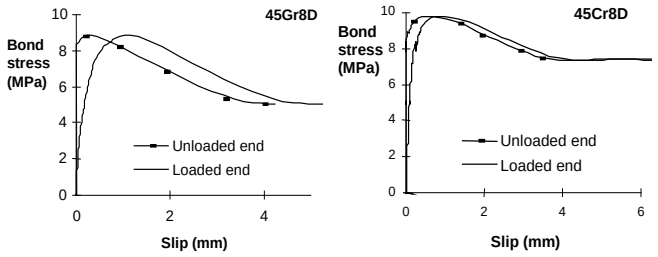

Fig. 4—Typical bond - slip envelopes for GFRP and CFRP embedments

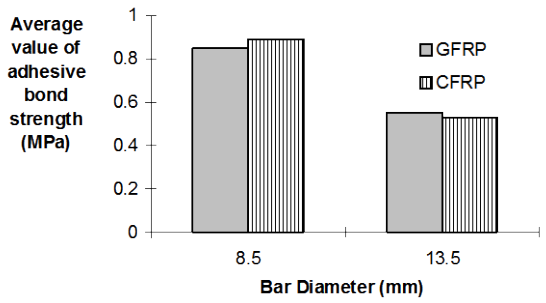

Fig. 5 Average values of adhesive bond strength with respect to the bar type and diameter

Fig. 6—GFRP specimen after the test

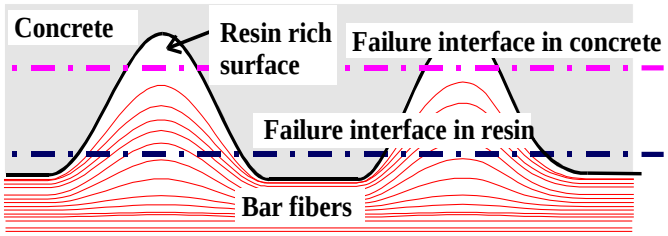

Fig. 7— Shear failure at the surface layer of FRP bars

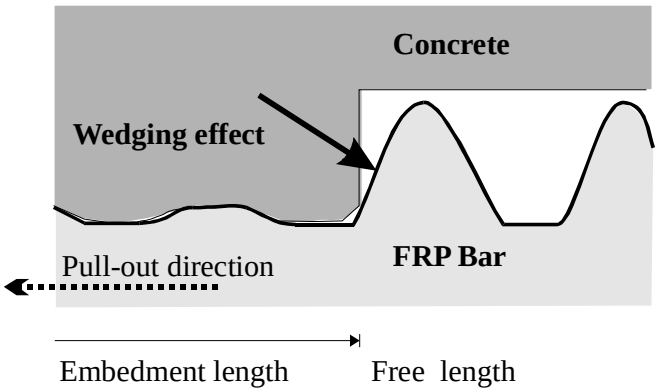

Fig. 8—The wedging action by the undamaged part of the bar

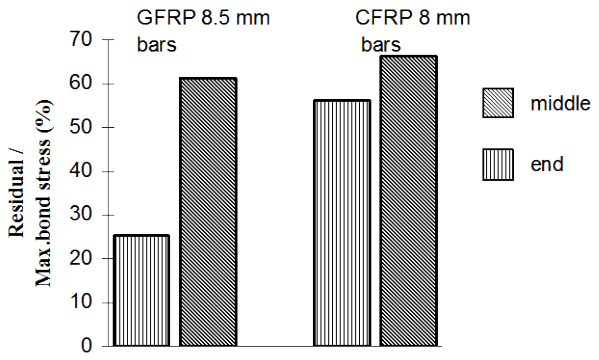

Fig. 9—Ratio of residual to maximum bond stress for round FRP bars

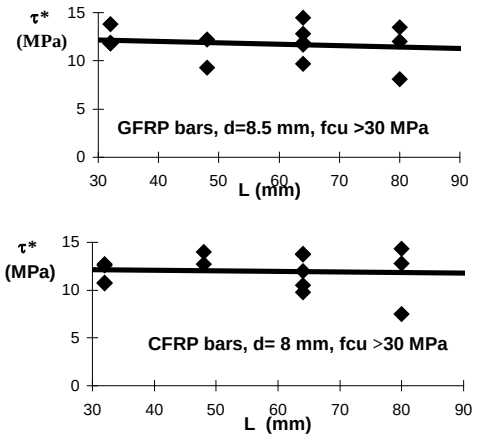

Fig. 10—Bond stress versus embedment length for GFRP and CFRP round bars

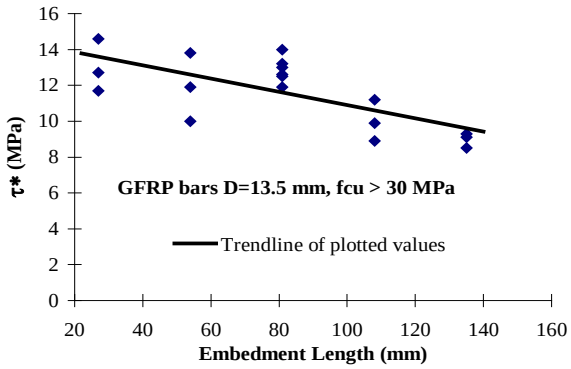

Fig. 11— Influence of embedment length on τ*

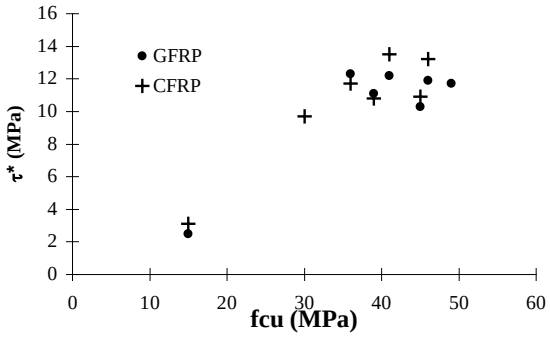

Fig. 12— Influence of concrete strength on τ* for FRP bars

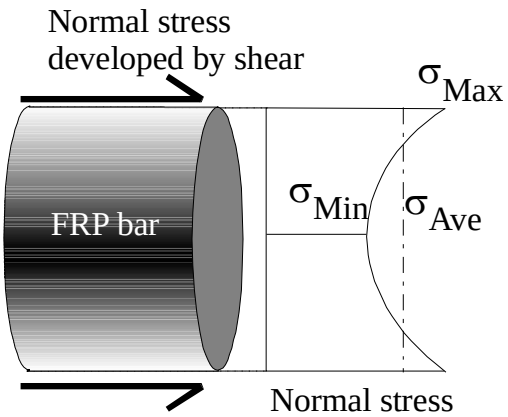

Fig. 13— Indicative distribution of normal stresses on a FRP bar cross-section subjected to axial load

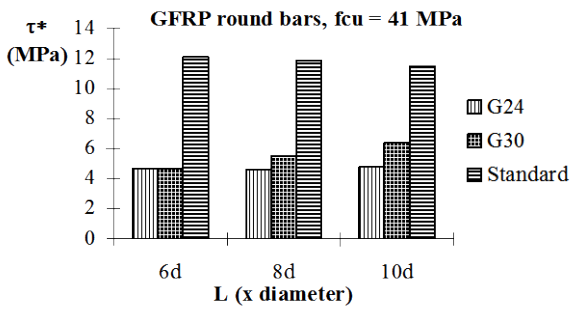

Fig. 14— Bars with different type of surface deformations